Inorganic Chemistry

Article

pubs.acs.org/IC

Highly Selective Colorimetric and Luminescence Response of a Square-Planar Platinum(II) Terpyridyl Complex to Aqueous TcO_4^-

Sayandev Chatterjee,*[,†] Amie E. Norton,[‡] Matthew K. Edwards,[†] James M. Peterson,[†] Stephen D. Taylor,[‡] Samuel A. Bryan,[†] Amity Andersen,[§] Niranjan Govind,[§] Thomas E. Albrecht-Schmitt,[∥] William B. Connick,*[,‡] and Tatiana G. Levitskaia*[,†]

[†]Energy and Environment Directorate, Pacific Northwest National Laboratory, Richland, Washington 99354, United States

[‡]Department of Chemistry, University of Cincinnati, Cincinnati, Ohio 45221, United States

[§]Environmental & Molecular Sciences Laboratory, Pacific Northwest National Laboratory, Richland, Washington 99354, United States

[∥]Department of Chemistry and Biochemistry, Florida State University, Tallahassee, Florida 32306, United States

Supporting Information

ABSTRACT: Molecular recognition of an aqueous pertechnetate (TcO_4^-) anion is fundamentally challenging partly due to the charge-diffuse nature of this anion, which hampers design of new technologies for its separation and detection. To address this gap, simple salts of transition metal complexes that undergo a distinct spectroscopic change upon exposure to aqueous anions were explored. The Pt(II) complex [Pt(tpy)-Br]SbF_6 (tpy = 2,2′;6′,2″-terpyridine) undergoes a dramatic color change and intense luminescence response upon TcO_4^- uptake due to concomitant enhancement of Pt···Pt interactions. The spectroscopic response was highly selective and quantitative for aqueous TcO_4^- among other competing anions. Complementary Raman spectroscopy and microscopy techniques, structural determination, and theoretical methods were employed to elucidate the mechanism of this response at the molecular level.

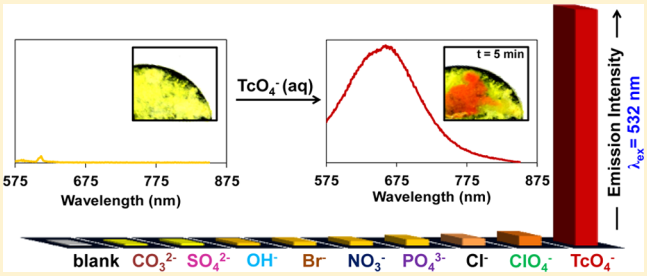

INTRODUCTION

Over the last several decades, significant progress in the recognition and sensing of anionic species has been achieved;[1−8] however, their selective separation and detection in complex multicomponent matrices ranging from biological systems to hazardous waste remains challenging. Of particular interest is recognition of toxic and/or radioactive anionic species such as TcO_4^-, the most dominant environmental chemical form of the radioisotope ^{99}Tc produced in the nuclear fuel cycle. The long half-life of ^{99}Tc (2.13×10^5 years) and highly mobile subsurface transport properties of $^{99}TcO_4^-$ generate considerable environmental and health concerns. Monitoring of ^{99}Tc in the groundwater is challenging due to the requirement to meet low detection limits below the drinking water standard. The very few commercially deployable methods for the sensitive, rapid, on-site detection of TcO_4^- presently available typically rely on complex sample treatment involving separation and preconcentration steps using anion exchange resins with scintillating properties followed by the radiometric determination.[9−11] Generally, these techniques have a low counting efficiency due to the color-quenching effects of several compounds potentially present in groundwater and removed by the ion exchange substrate such as chromate and certain organics.

A recently proposed spectroelectrochemical method may offer a solution to the aforementioned issues, by providing rapid and selective TcO_4^- detection.[12−14] This sensor technique relies on charge selective preconcentration of TcO_4^- within a polymeric film, followed by electrochemical Tc(VII) reduction and its subsequent *in situ* complexation to generate a species with a unique luminescent signature. While this process is capable of highly selective TcO_4^- detection even in the presence of interfering species, it is challenging due to several factors including the limited number of well-characterized luminescent low-valent Tc complexes[13,15−22] and the difficulties associated with the generation and subsequent detection of the luminescent Tc species in the film matrix in contact with multicomponent solutions that can quench the luminescence response. Development of an alternative approach involving molecular recognition would be highly advantageous for the detection and sequestration of the anions of interest in complex multicomponent matrices by reducing matrix effects and improving detection selectivity.

Design of selective receptors that are useful for practical sensing and/or sequestration of TcO_4^- has proven to be challenging partly due to the charge-diffuse nature of this large

Received: July 26, 2015
Published: October 8, 2015

ACS Publications © 2015 American Chemical Society

DOI: 10.1021/acs.inorgchem.5b01664
Inorg. Chem. 2015, 54, 9914−9923

Scheme 1. Schematic Illustrating the Change in Pt···Pt Interactions Due to a Simple X^-/Y^- Anion Exchange

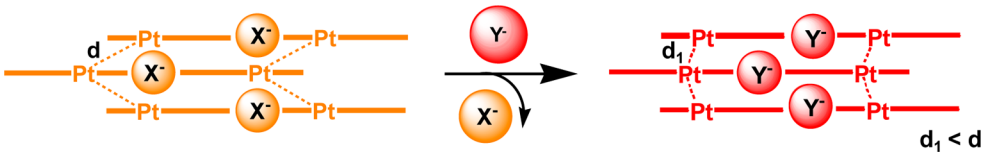

anion. Hydrogen-bond donor host molecules commonly used for anion recognition and sensing exhibit poor affinity for TcO_4^- in comparison with small charge dense anions.[23] The problem of overcoming this bias relies on the receptors incorporating several design criteria. One representative example exploits the spatial complementarity between TcO_4^- and the inclusion cavity of a cryptand receptor leading to the rare precedent of selective recognition of TcO_4^- in aqueous solution over NO_3^- and Cl^- anions as evaluated by ^{99}Tc NMR spectroscopy. However, the sensitivity of the cryptand to ClO_4^- and other tetrahedral, singly charged oxoanions other than the structural surrogate ReO_4^- was not reported.[24] One practical drawback of these molecular recognition receptors is related to their typically elaborate synthesis and purification.

In an effort to take advantage of the selectivity benefits associated with the molecular recognition approach, we have evaluated the response to TcO_4^- of readily available transition metal complexes that undergo a distinct spectroscopic change upon exposure to aqueous anions such as ClO_4^-.[25] To this end, application of coordinatively unsaturated Pt(II) salts as the colorimetric materials for the selective recognition of aqueous anions, and TcO_4^- in particular, is motivated by the several considerations. Square-planar Pt(II) complexes with sterically permitting ligands are capable of forming quasi-one-dimensional stacked systems via noncovalent Pt···Pt interactions.[26−30] These systems exhibit rich spectroscopic properties that are modulated by changing the Pt···Pt interactions.[31,32] This tuning can be achieved by varying the nature of the ligands and/or counteranion.[33−36] In a parent solid material, the square-planar Pt(II) units are arranged in a manner that does not result in a continuous chain of short Pt···Pt contacts. Substitution of an anion (or introduction of a solvate), whose chemical nature, electronic structure, and geometry uniquely satisfy the requirements of the new lattice parameters needed for extended Pt···Pt overlap (as shown in Scheme 1), will result in distinct changes in spectroscopy of the parent material. These spectroscopic changes form the basis of detection of the analyte.

The spectroscopy of Pt(II) compounds has long served as a signature for weak noncovalent Pt···Pt interactions in the solid state that lead to shortening of Pt···Pt distances.[37,38] The susceptibility of the Pt···Pt interactions in these systems to changes in the molecular environment has been extensively documented with considerable emphasis on the response of these materials to neutral molecules, such as organic vapors. Vapor absorption induces significant changes in Pt···Pt interactions in these systems, causing pronounced changes in spectroscopic properties.[39−45] Similarly, the counteranion characteristics affect the crystal lattice of Pt(II) complexes including Pt···Pt distances, and the concomitant spectroscopic properties can be utilized for the anionic substrate detection, which to date has received only limited consideration.[35,46−50] We have recently demonstrated that highly selective recognition of aqueous ClO_4^- anion by $[Pt(tpy)Cl](PF_6)$ can be achieved by this approach.[25] The exchange of PF_6^- anions by aqueous ClO_4^- forces the $[Pt(tpy)Cl]^+$ units into a stacked columnar arrangement, arranged intermittently between channels occupied by hydrogen-bonded $ClO_4^-\cdots H_2O$ networks. This synergistic effect of the hydrated anion results in extended Pt···Pt interactions stabilizing the MMLCT transition and generates strong luminescence response that is key to aqueous ClO_4^- detection. In this work, we demonstrate the selective detection of the aqueous TcO_4^- using solid $[Pt(tpy)Br](SbF_6)$ (**1**·SbF_6). Theoretical calculations performed on both $[Pt(tpy)Cl](PF_6)/ClO_4^-$ and $[Pt(tpy)Cl](PF_6)/TcO_4^-$ systems provide insights into the mechanism of the spectroscopic response.

EXPERIMENTAL DETAILS

Radiation safety disclaimer! *Technetium-99 has a half-life of 2.12 × 10^5 years and emits a low-energy (0.292 MeV) β particle; common laboratory materials provide adequate shielding. Normal radiation safety procedures must be used at all times to prevent contamination.*

Reagents and Materials. $KTcO_4$ and NH_4TcO_4 were in-house stocks available at the Radiochemical Processing Laboratory at the U.S. Department of Energy Pacific Northwest National Laboratory, Richland, WA. K_2PtCl_4 was purchased from Pressure Chemical. 1,5-Cyclooctadiene (COD) and 2,2′:6′2″-terpyridine (tpy) were obtained from Sigma-Aldrich. $KSbF_6$ and dichloromethane were purchased from Alfa Aesar. Reaction grade $NaClO_4$, Na_2SO_4, NaCl, NaBr, LiBr, NaOH, Na_2CO_3, $NaNO_3$, $NaClO_4$, and $Na_3PO_4·10H_2O$ were purchased from Fischer Scientific. Na_2CrO_4, Na_2IO_4, Na_2ReO_4, and $Na_2MnO_4·H_2O$ were purchased from Sigma-Aldrich. Starting material $Pt(COD)Cl_2$ was prepared according to the published procedure.[51] $Pt(COD)Br_2$ was prepared by adding excess equivalents of LiBr to a dichloromethane solution of $Pt(COD)Cl_2$. $[Pt(tpy)Br]Br·2H_2O$ was prepared according methods adapted from published procedures for the synthesis of [Pt(tpy)Cl]Cl.[52] Vycor porous glass rods (4 in. × 0.112 in.) were purchased from Advanced Glass and Ceramics and cut into 0.125 in. long beads.

Synthesis and Characterization of Platinum(II) Salts. $[Pt(tpy)Br](SbF_6)$ (**1**·SbF_6) was prepared through anion metathesis, by adding a saturated aqueous solution of $KSbF_6$ to an aqueous solution of $[Pt(tpy)Br]Br·2H_2O$ according to a known procedure.[53] In a typical metathesis, 5 mL of saturated aqueous $KSbF_6$ solution was added to 0.622 g of $[Pt(tpy)Br]Br·2H_2O$ (1.0 mmol) dissolved in 10 mL of deionized (DI) water. A yellow precipitate formed immediately. The solution was allowed to sit for 10 min to allow complete precipitation, and the solid was collected by filtration followed by washing with diethyl ether. Yield = 87%. Anal. Calcd for $C_{15}H_{11}N_3BrF_6SbPt$: C, 24.22; H, 1.49; N, 5.65. Found: C, 24.25; H, 1.45; N, 5.63. ^1H NMR (400 MHz, CD_3CN, δ) 9.3 (2H, d with Pt satellites J_{H-Pt} = 37 Hz, J_{H-H} = 5.6 Hz, CH), 8.50 (1H, t, J_{H-H} = 8.0 Hz, CH), 8.37 (2H, dd, J_{H-H} = 8.0 and 7.6 Hz, CH), 8.3−8.2 (4H, m, CH), 7.83 (2H, dd, J_{H-H} = 8.0 and 7.6 Hz, CH). MS-ESI (positive ion mode, CH_3CN) (*m*/*z*): 506.0 ($Pt(tpy)Br^+$). MS-ESI (negative ion mode, CH_3CN) (*m*/*z*): 234.9 (SbF_6^-).

$[Pt(tpy)Br](TcO_4)$ (**1**·TcO_4) was prepared through anion metathesis following a method similar to that used in the synthesis of **1**·SbF_6, by adding 1 mL of 10.0 mM aqueous solution of NH_4TcO_4 to 0.062 g of $[Pt(tpy)Br]Br·2H_2O$ (0.10 mmol) dissolved in 1 mL of DI water. An orange precipitate formed immediately. The solution was allowed to sit for 10 min to allow complete precipitation, and the precipitate was collected by filtration followed by washing with diethyl

DOI: 10.1021/acs.inorgchem.5b01664
Inorg. Chem. 2015, 54, 9914−9923

ether and dried under air to yield a yellow solid. Yield = 79%. MS-ESI (positive ion mode, CH_3CN) (m/z): 506.0 ($Pt(tpy)Br^+$). MS-ESI (negative ion mode, CH_3CN) (m/z): 162.9 (TcO_4^-).

[Pt(tpy)Br](TcO_4·xH_2O) (**1**·TcO_4·xH_2O) was prepared by contacting water with the yellow **1**·TcO_4 crystals to form an orange-red precipitate.

[Pt(tpy)Br](AsF_6) (**1**·AsF_6) was prepared through anion metathesis, following a method similar to that used in the synthesis of **1**·SbF_6 where 5 mL of saturated aqueous solution of $KAsF_6$ was added to 0.622 g of [Pt(tpy)Br]Br·$2H_2O$ (1.0 mmol) dissolved in 10 mL of DI water. A yellow precipitate formed immediately. The solution was allowed to sit for 10 min to allow complete precipitation, and the precipitate was collected by filtration followed by washing with diethyl ether. Yield = 91%. Anal. Calcd for $C_{15}H_{11}N_3BrF_6AsPt$: C, 25.84; H, 1.59; N, 6.03. Found: C, 25.83; H, 1.61; N, 6.03. ^1H NMR (400 MHz, CD_3CN, δ) 9.3 (2H, d with Pt satellites J_{H-Pt} = 37 Hz, J_{H-H} = 4.8 Hz, CH), 8.50 (1H, t, J_{H-H} = 8.0 Hz, CH), 8.37 (2H, dd, J_{H-H} = 8.0 and 7.6 Hz,CH), 8.3−8.2 (4H, m, CH), 7.82 (2H, dd, J_{H-H} = 8.0 and 7.6 Hz,CH). MS-ESI (positive ion mode, CH_3CN) (m/z): 506.0 ($Pt(tpy)Br^+$). MS-ESI (negative ion mode, CH_3CN) (m/z): 188.9 (AsF_6^-).

Characterization Techniques. UV−vis absorption spectra were recorded using a Varian Cary 50Bio UV−vis absorption spectrophotometer. Emission and excitation spectra were recorded using a Horiba Fluorolog III fluorimeter equipped with a 450 W xenon lamp and a R928 Hamamatsu photomultiplier tube. Spectra were not corrected for instrument response. For powder samples or aqueous suspensions, the samples were taken in 2 mm × 4 mm quartz cuvettes. For measurements involving Vycor beads, the beads were carefully positioned to ensure that the optical paths remained essentially unchanged.

Raman spectroscopy measurements were carried out using a Renishaw inVia imaging microscope system. Spectra were obtained using 670 nm laser irradiation on samples in silica cells. Scanning electron microscopic (SEM) images were recorded using FEI Quanta 250 field emission microscope. Aqueous suspensions of **1**·SbF_6 and **1**·TcO_4·xH_2O were deposited onto a circular carbon film (2 cm diameter) mounted on an aluminum support. The powder X-ray diffraction (XRD) patterns were obtained using a Bruker Advance instrument (Cu Kα radiation λ = 1.5418 Å) equipped with a graphite monochromator. Data were collected in a step scan mode between 5° and 70° 2θ, with a step size of 0.0148° and time per step of 0.3 s. The data were analyzed using Jade MDI software.

Crystal Structure Determination. A single crystal of **1**·TcO_4 was glued to a Mitogen mount with epoxy and optically aligned on a Bruker D8 Quest X-ray diffractometer using a digital camera. Initial intensity measurements were performed using an IμS X-ray source (Mo Kα, λ = 0.710 73 Å) with high-brilliance and high-performance focusing multilayered optics. Standard Quest software was used for determination of the unit cells and data collection control. The intensities of reflections of a sphere were collected by a combination of multiple sets of exposures (frames). Each set had a different φ angle for the crystal, and each exposure covered a range of 0.5° in ω. SAINT software was used for data integration including Lorentz and polarization corrections. Crystals of [Pt(tpy)Br](TcO_4) were non-merohedrally twinned with a rotation angle of 180°. The program CELL_NOW was used to index the two twin domains. Standard Quest software was used to integrate the twin domains, and multiscan absorption corrections were applied using the program TWINABS. The structure was solved by direct methods and refined on F^2 by full-matrix least-squares techniques using the program suite SHELX. Crystallographic data summary is included in Supporting Information (Table S1). Atomic coordinates and additional structural information are provided in the Supporting Information (CIF).

Theoretical Methods. Ground state density functional theory (DFT) calculations were performed to optimize the crystal structures using a plane-wave basis set, Vanderbilt ultrasoft pseudopotentials,[54] with the Quantum-Espresso electronic structure code.[55] Starting structures for the **1**·SbF_6 and **1**·TcO_4 complexes were taken from the literature[53] and this work, respectively. Energy cutoff for the plane-wave basis set was set at 35 Ry, and the Brillouin zone for the systems of interest were sampled with the Monkhorst−Pack scheme:[56] 3 × 2 × 2 and 4 × 2 × 1 k-point grids for the **1**·SbF_6 and **1**·TcO_4 complexes, respectively. The PBE exchange-correlation functional[57] in combination with the Grimme dispersion correction[58] was used for all ground state calculations. As the structure of **1**·TcO_4·xH_2O is unknown, the [Pt(tpy)Cl]ClO_4·H_2O structure was used as a template for a hypothetical hydrous [Pt(tpy)Br]TcO_4·H_2O to get a qualitative estimation of the influence of water on the electronic structure of the complex.

Following the crystal structure optimizations, aligned trimer cluster models that demonstrate the essential Pt···Pt interactions were extracted from the crystal structure models. Excited state time-dependent DFT (TDDFT) calculations (without spin−orbit effects) were performed on these cluster models to simulate the UV−vis spectra of the **1**·SbF_6 and **1**·TcO_4·xH_2O complexes. All TDDFT calculations were performed with the PBE0 exchange-correlation functional[59] with the 6-31G** basis set for the light atoms, C, N, O, F, P, Cl, and H,[60,61] and the Stuttgart basis set and scalar relativistic effective core potential (ECP) for the heavier atoms, Sb, Br, Tc, and Pt.[62,63] These calculations were performed with the NWChem electronic structure program.[64]

Quantitative Determination of TcO_4^-. For quantitative determination of the aqueous TcO_4^- in aqueous solutions and the detection selectivity, **1**·SbF_6 or **1**·TcO_4·xH_2O were supported on Vycor glass beads by sonicating dried porous glass beads in solutions of 20 mg of each complex in 2 mL of 50% w/w DMSO/acetone solution for several hours. The beads were removed from solution, washed with water, air-dried, weighed to determine amount of loading of platinum complex, and stored in a closed vial until further use. For the quantification of aqueous TcO_4^- uptake, a calibration plot was generated placing Vycor porous glass platforms loaded with **1**·SbF_6 in the aqueous solution containing 1.0 mM aqueous solutions of sodium salts of TcO_4^-, ReO_4^-, IO_4^-, ClO_4^-, MnO_4^-, CrO_4^{2-}, Cl^-, PO_4^{3-}, NO_3^-, Br^-, OH^-, CO_3^{2-}, or SO_4^{2-} for 1 h. Subsequently, the beads were washed with water, wiped dry, and subjected to spectroscopic measurements.

For generation of the TcO_4^- calibration plot, DI water spiked with varying concentrations of TcO_4^- ranging from 3.8 × 10^{-12} to 3.8 × 10^{-6} M was used. Vycor beads loaded with **1**·SbF_6 (~2% by weight) were immersed in these solutions for 1 h. Emission spectra were collected upon excitation at 532 nm. From the plot of emission intensity versus the logarithm of the aqueous TcO_4^- concentration, a preliminary value of the detection limit was calculated as recommended by the International Union of Pure and Applied Chemistry (IUPAC)[65] using eq 1:

$$\mathrm{DL} = \frac{kS_b}{m} \tag{1}$$

Here, DL is the detection limit, k is a numerical constant, m is the slope of the linear region of the plot, and S_b is the standard error for the blank measurements, respectively. Emission spectra of Vycor porous glass beads immersed in DI water for 1 h upon excitation at 532 nm were used for blank measurements. In accord with IUPAC recommendations, a k value of 3 was applied, which corresponds to a 99.87% confidence level.

To test the ability of the sensor to detect aqueous TcO_4^- from groundwater, groundwater collected from the well 299-W19-36 at the Hanford site in Washington was used. The major inorganic constituents present in the groundwater are listed in Table S2, Supporting Information.[66] The water was spiked with different concentrations of TcO_4^- ranging from 7.5 × 10^{-8} to 7.5 × 10^{-6} M. **1**·SbF_6 supported Vycor beads were immersed in these solutions for 1 h.

RESULTS AND DISCUSSIONS

Colorimetric Response of 1·SbF_6 to Aqueous TcO_4^-. Compound **1**·SbF_6 (Scheme 2) exhibits negligible solubility in water and readily crystallizes from aqueous acetone solutions as

DOI: 10.1021/acs.inorgchem.5b01664
Inorg. Chem. 2015, 54, 9914−9923

Scheme 2. Conversion of Yellow [Pt(tpy)Br]SbF_6 (1·SbF_6) to Red [Pt(tpy)Br]TcO_4·xH_2O (1·TcO_4·xH_2O) on Exposure to Aqueous TcO_4^-

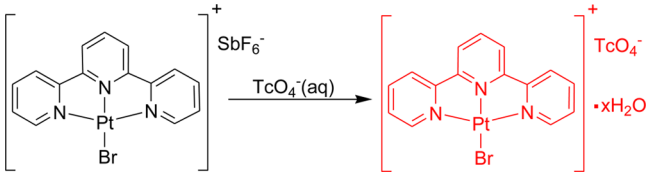

yellow needles. To assess its colorimetric response to TcO_4^-, a yellow microcrystalline powder (~10 mg) or aqueous suspension (~10 mg in 1 mL of DI water) of 1·SbF_6 was exposed to 50 μL of 1.0 mM aqueous solution of TcO_4^-. A distinct color change from yellow to red was observed within 2–5 min. Results were indistinguishable irrespective of whether $KTcO_4$ or NH_4TcO_4 was used as the source of TcO_4^-. The presence of water is a key factor in the color change; this is exemplified by the observation that when the 1·SbF_6 powder treated with aqueous TcO_4^- solution was allowed to dry, it changed from red back to yellow. The behavior is reminiscent of yellow [Pt(tpy)Cl]ClO_4, which reversibly absorbs water vapor to form red [Pt(tpy)Cl]ClO_4·H_2O; the color of the latter is a direct consequence of a continuous chain of short Pt···Pt contacts (3.3031(5), 3.3692(5) Å) that result in a low-lying charge-transfer absorption band (*vide infra*).[25,67] By analogy, the sensitivity of yellow 1·TcO_4 to moisture is attributed to the incorporation of hydration water molecules in the crystal lattice of 1·TcO_4 leading to the structural reorganization and shortening of Pt···Pt distances. The concomitant enhancement of Pt···Pt interaction results in the stabilization of the MMLCT band and generates the red material.

To visually demonstrate the response of 1·SbF_6 to TcO_4^-, a circular carbon film was divided into three segments. 1·SbF_6 was deposited on two segments (marked 1 and 3 in Figure 1), whereas 1·TcO_4·xH_2O was deposited on segment 2. Details of the process are described in the Supporting Information. A drop of aqueous TcO_4^- solution (1 mM) was placed on top of 1·SbF_6 in segment 3. The platform was gently tilted to allow the drop to travel over the segment. It is seen that the color gradually changed from yellow to red wherever the drop made contact with the 1·SbF_6 (photos in Figure 1b–d were taken within 1, 2, and 5 min, respectively, of adding the drop). SEM images and elemental mapping of segment 3 confirm uptake of TcO_4^-, resulting in a morphology that is different from the 1·SbF_6 and 1·TcO_4·xH_2O coated segments 1 and 2 (Figure S1).

Crystal Structure of 1·TcO_4. Light orange-yellow needles of 1·TcO_4 grown from DMSO belong to the $P\bar{1}$ space group. There are two formula units in the asymmetric unit, and the [Pt(tpy)Br]$^+$ molecules (Figure 2) have distances and angles very similar to those of 1·SbF_6 and other reported Pt(tpy)X^+ complexes.[2−11] The approximately planar cations stack in columns parallel to *a*-axis. Each complex is canted such that the normal to its plane forms an angle of ~15° with the stacking axis, which results in interplanar spacings of ~3.36 Å. Viewed roughly perpendicular to planes of the molecules, consecutive complexes appear rotated by ~133.5°. Within the stacks, there are alternating short (3.460(3) Å) and long (3.975(3) Å) Pt··· Pt separations with Pt···Pt···Pt angles of 136.7(5)°. The absence of a more linear arrangement of closely spaced Pt centers is consistent with the yellow color of this crystal form.

Response of 1·SbF_6 to Aqueous TcO_4^- Exposure. *Raman Spectroscopy and X-ray Diffraction.* Raman spectra of a yellow 1·SbF_6 powder sample showed Sb–F vibrational bands at 280 and 654 cm^{-1}.[68,69] On the other hand, the red 1·TcO_4·xH_2O material gave rise to characteristic Tc–O vibrational bands at 909 and 325 cm^{-1} (Figure S2, Supporting Information) that are slightly shifted from the corresponding bands of solid NH_4TcO_4 or NBu_4TcO_4 (905, 321 cm^{-1}).[70] The 1·SbF_6 powder sample exposed to 1.0 mM NH_4TcO_4 for 3 h also exhibited Tc–O vibrational bands at 909 and 325 cm^{-1}, in addition to Sb–F vibrational bands,[68,69] suggesting that 1·SbF_6 exposure to aqueous TcO_4^- results in partial conversion to 1·TcO_4·xH_2O. This conclusion was confirmed by X-ray diffractograms of the 1·SbF_6 powder sample exposed to aqueous TcO_4^- showing the presence of phases corresponding to both 1·SbF_6 starting material and the independently prepared 1·TcO_4·xH_2O product (Figure S3).

UV–Vis Spectroscopic Response and Electronic Structure. The absorption spectrum of the 1·SbF_6 loaded on the Vycor beads (Figure 3A) shows an intense transition near 340 nm, which has been assigned to the spin-allowed tpy-centered ($^1LC_1$) π–π^* transition.[33] However, as first noted by Che and co-workers,[71] the energy and Franck–Condon factors of bands in this region are very sensitive to changes in the ancillary ligand, thereby establishing that these transitions are not purely ligand centered. This behavior has been attributed to mixing between LC and low-lying metal-to-ligand charge-transfer (^{1}MLCT) states. A spin-allowed 5d(Pt) → π^*(tpy) metal-to-ligand charge-transfer transition (MLCT) transition characteristic of the Pt(tpy)Br^+ chromophore is observed near 400 nm, that tails to longer wavelengths (Figure 3A).[71] Immersion of the 1·SbF_6-loaded glass beads in 1.0 mM aqueous NH_4TcO_4 solution resulted in the appearance of a new band at longer wavelength, as shown in Figure 3A, inset. The band is nearly identical to that observed when beads are loaded with 1·TcO_4·xH_2O (Figure 3A) and is attributed to a metal–metal-to-ligand charge-transfer MMLCT [dσ^*(Pt)–π^*(tpy)] transition where

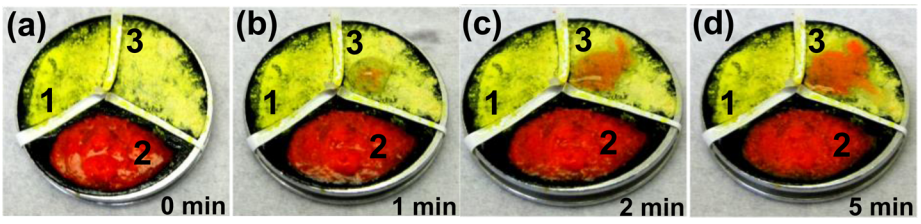

Figure 1. Photographs illustrating the kinetics of 1·SbF_6 response to aqueous TcO_4^-. Segments 1 and 3 are coated with 1·SbF_6, while segment 2 is coated with 1·TcO_4·xH_2O. (a) t = 0. (b) A drop of TcO_4^- solution is placed on top of segment 3, which starts developing red color (t = 1 min). (c) As the platform is gradually tilted toward segment 3, the red color spreads along with the drop (t = 2 min). (d) The red color in segment 3 maps out the path of the drop (t = 5 min).

DOI: 10.1021/acs.inorgchem.5b01664
Inorg. Chem. 2015, 54, 9914–9923

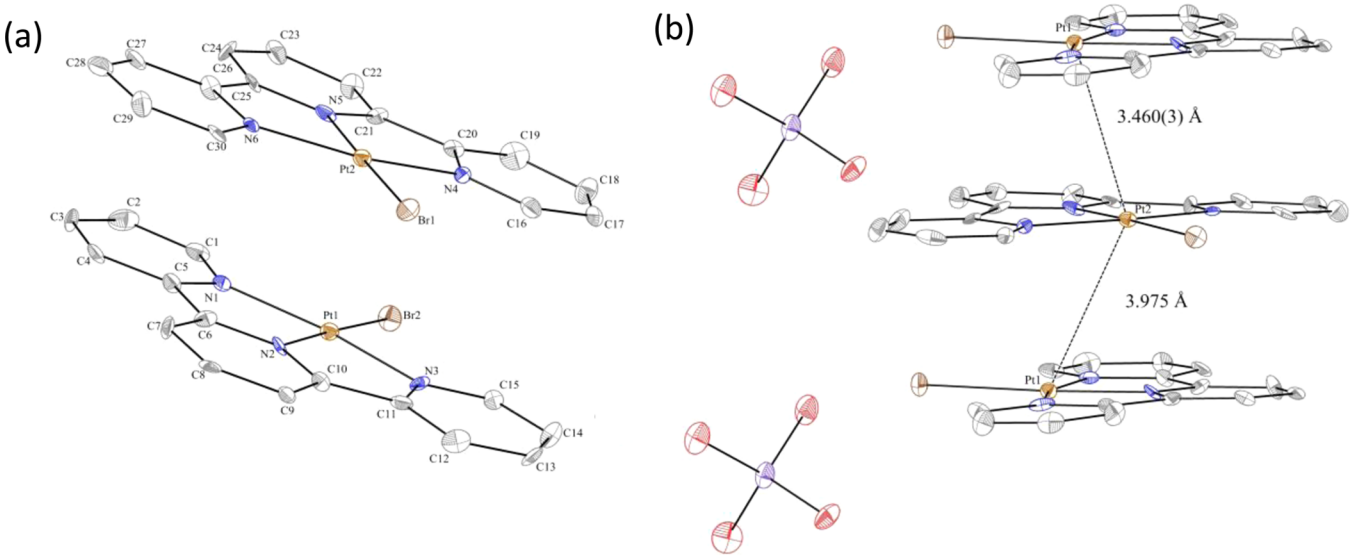

Figure 2. Crystal structure of $1{\cdot}TcO_4$: (a) the unit cell with $[Pt(tpy)Br]^+$ units and (b) the stacking of $[Pt(tpy)Br]^+$ units with Pt···Pt distances in angstroms. H-atoms have been omitted for clarity (thermal ellipsoids at 50% probability).

Table 1. Selected Distances (Å) and Angles (deg) for $1{\cdot}TcO_4$

Distances (Å)	
Pt1−Br2	2.423(2)
Pt1−N1	2.032(8)
Pt1−N2	1.945(9)
Pt1−N3	2.006(9)
Pt1−Pt2	3.460(3)
Pt2−Br1	2.420(2)
Pt2−N4	2.031(9)
Pt2−N5	1.945(9)
Pt2−N6	2.027(8)
Pt1−Pt2	3.460 (3)
Angles (deg)	
N1−Pt1−N2	81.33(4)
N2−Pt1−N3	80.93(4)
N1−Pt1−N3	162.3(4)
Br2−Pt1−N1	98.7(3)
Br2−Pt1−N2	177.7(3)
Br2−Pt1−N3	99.0(3)
N4−Pt2−N5	81.6 (4)
N5−Pt2−N6	80.5 (4)
N4−Pt2−N6	162.0 (4)
Br1−Pt2−N4	98.8 (2)
Br1−Pt2−N5	178.3 (3)
Br1−Pt2−N6	99.11 (3)
Br1−Pt2−Pt1−Br2	133.2(1)

the $d\sigma^*$ arises from the interaction of the d_{z^2}(Pt) orbitals of adjacent complexes.[26,31,33,39,41]

Using 415 nm laser excitation, emission studies were performed on powder samples of yellow crystals of $1{\cdot}SbF_6$ and orange-yellow crystals of $1{\cdot}TcO_4$ as well as yellow aqueous suspensions of $1{\cdot}SbF_6$ and red aqueous suspensions of $1{\cdot}TcO_4{\cdot}xH_2O$. The yellow crystalline powders of $1{\cdot}SbF_6$ exhibit an intense emission at ∼555 nm. The emissions of yellow crystals of $1{\cdot}SbF_6$, orange-yellow crystals of $1{\cdot}TcO_4$, and red aqueous suspensions of $1{\cdot}TcO_4{\cdot}xH_2O$ are shown in Figure 3B. The emission spectrum remains unchanged for the $1{\cdot}SbF_6$ powders in contact with water and is therefore not shown separately; this suggests that no chemistry or change in the electronic structure of the complex occurs upon water exposure. Likewise, the emission from orange-yellow crystalline needles of $1{\cdot}TcO_4$ is very similar, exhibiting a maximum at ∼562 nm. On the other hand, contact of $1{\cdot}TcO_4$ with water generates red $1{\cdot}TcO_4{\cdot}xH_2O$. The emission from the latter material is strongly red-shifted, exhibiting a maximum near ∼590 nm (Figure 3B). The shift to longer wavelengths is suggestive of emission originating from the lowest, predominantly spin-forbidden, MMLCT excited state,[34,35,72−74] which is strongly dependent on the Pt···Pt separation. In other words, the data are consistent with water absorption causing a shortening of the Pt···Pt distances. In keeping with this assignment, we note that the excitation spectra of the red $1{\cdot}TcO_4{\cdot}xH_2O$ samples show a band near 540 nm, which is attributed to a spin-allowed MMLCT transition (Figure S4). The longest wavelength feature in the spectra of $1{\cdot}SbF_6$ and dry orange-yellow needles of $1{\cdot}TcO_4$ occurs at much shorter wavelengths (∼500 nm), as expected for longer Pt···Pt distances in those materials.

Emission studies performed using 532 nm light demonstrate that $1{\cdot}TcO_4{\cdot}xH_2O$ can be selectively excited at this wavelength (Figure 3C). Under these conditions, yellow $1{\cdot}SbF_6$ powder and aqueous suspensions are essentially nonabsorbing and consequently exhibited extremely weak emissions. A powdered sample of anhydrous yellow-orange needles of $1{\cdot}TcO_4$ also showed a very weak emission with only slightly higher emission intensity (λ_{max} ∼ 575 nm) compared to yellow powders of $1{\cdot}SbF_6$. On the other hand, when excited at 532 nm, the red aqueous suspension of $1{\cdot}TcO_4{\cdot}xH_2O$ displayed an intense emission at 592 nm (Figure 3C). Exposure of a powder sample of $1{\cdot}SbF_6$ to the aqueous solution of 1.0 mM NH_4TcO_4 for 30 min resulted in a similar emission spectrum.

Additional experimentation indicates that not every platinum salt can be used for the detection of aqueous TcO_4^-. Several platinum(II) salts (e.g., [Pt(tpy)Cl]OTf, [Pt(tpy)Cl]Cl, [Pt(tpy)I]I, and $1{\cdot}AsF_6$) were exposed to 10 mM aqueous TcO_4^- (OTf = triflate). Only $1{\cdot}SbF_6$ was observed to provide a unique, prominent, and distinguishable luminescent signature upon exposure to aqueous TcO_4^-. For example, [Pt(tpy)Cl]OTf, [Pt(tpy)Cl]Cl, and [Pt(tpy)I]I were found to show no

DOI: 10.1021/acs.inorgchem.5b01664
Inorg. Chem. 2015, 54, 9914−9923

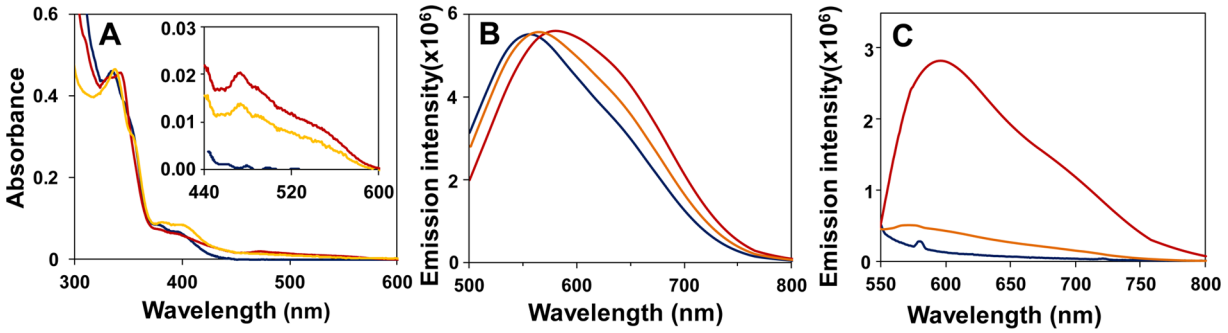

Figure 3. (A) Absorption spectra of $Pt(tpy)Br^+$ salts loaded into Vycor beads: (blue) **1**·SbF_6, (red) **1**·TcO_4·xH_2O, (yellow) **1**·SbF_6 exposed to 1.0 mM TcO_4^- for 3 h. Inset: The longer wavelength absorption magnified. (B, C) Emission spectra of (blue) dry yellow powder of **1**·SbF_6, (orange) dry orange powder of **1**·TcO_4, (red) red aqueous suspension of **1**·TcO_4·xH_2O (B, λ_{ex} = 415 nm; C, λ_{ex} = 532 nm).

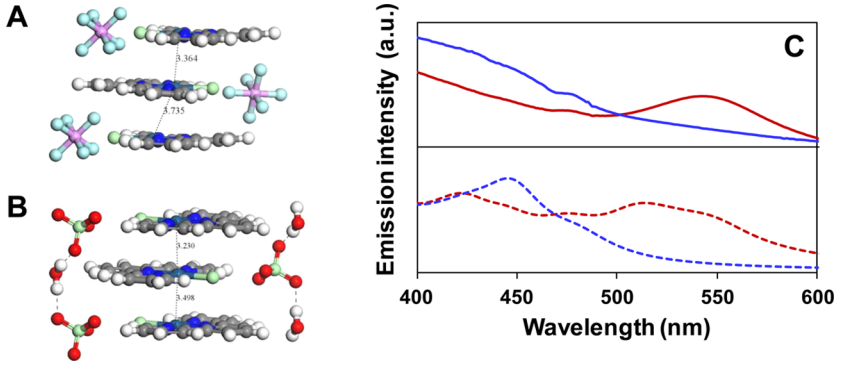

Figure 4. Trimer cluster models constructed from crystal lattice of previously published (A) $[Pt(tpy)Cl]PF_6$, (B) $[Pt(tpy)Cl]ClO_4$·H_2O. (C) Solid lines: Experimental absorption spectra of the $[Pt(tpy)Cl]^+$ systems. Dashed lines: TD-DFT simulated singlet absorption spectra from the trimer model systems. Blue line is for $[Pt(tpy)Cl]PF_6$ absorption, and red line is for $[Pt(tpy)Cl]ClO_4$·H_2O absorption.

response upon TcO_4^- exposure (Figures S5–S7, Supporting Information). The inability of similar materials with $[Pt(tpy)Cl]^+$ and $[Pt(tpy)I]^+$ backbones to produce similar changes upon aqueous TcO_4^- exposure highlights the importance of the ancillary bromide in the solid-to-solid transformation. Such specificity also has been noted for detection of aqueous ClO_4^- using $[Pt(tpy)Cl](PF_6)$.[25] Even for the analogous **1**·AsF_6 salt, the response was less dramatic and definitive. Unlike **1**·SbF_6 whose exposure to aqueous TcO_4^- "turns on" the emission upon 532 nm excitation, **1**·AsF_6 is already luminescent under these conditions, and a similar exposure merely shifts the emission to longer wavelengths (Figure S8, Supporting Information). In other words, **1**·AsF_6 absorbs at longer wavelengths than **1**·SbF_6. Assuming that the energy maxima of the lowest energy charge-transfer band can be used as a measure of the Pt···Pt interaction, this observation suggests that the increase in Pt···Pt interaction when TcO_4^- replaces AsF_6^- is less than when it replaces SbF_6^-. Moreover, we can speculatively suggest that Pt···Pt distances tend to decrease along the series [**1**·SbF_6] > [**1**·AsF_6] > [**1**·TcO_4·xH_2O]. The shortest Pt···Pt distances obtained from the crystal structures of **1**·SbF_6 and **1**·AsF_6 are consistent with this hypothesis ([**1**·SbF_6] = 3.49 Å; [**1**·AsF_6] = 3.39 Å).[53]

Theoretical Modeling of the Electronic Structures. In order to model the possible electronic structures of these materials, ground state DFT and excited state TDDFT calculations were performed. Initial calculations were conducted on the $[Pt(tpy)Cl](PF_6)/ClO_4^-$ system, which had been experimentally characterized in our previous work.[25] Stacked dimer and trimer models were considered for the $[Pt(tpy)Cl]PF_6$ and $[Pt(tpy)Cl]ClO_4$·H_2O, and the aligned trimer structure was determined to give the best representation of these systems. With this in mind, we used a trimer model for the brominated complexes, which will be described shortly. Upon replacement of the PF_6^- in $[Pt(tpy)Cl]PF_6$ (Figure 4A) with aqueous ClO_4^- (Figure 4B), the water molecules are observed to interact with the ClO_4^- ions to form a hydrogen-bonding network. This interaction orients the ClO_4^- ions in single channels, therefore aligning the Pt atoms, and shortening the Pt···Pt distances. This reduction of the Pt···Pt distances and the spatial alignment facilitate metal–metal-to-ligand charge-transfer.[25] Indeed, analysis of the orbitals involved in the electronic transition manifesting as the visible absorption band at 520 nm shows evidence of MMLCT. This transition originates from the occupied Pt 5d, O 2p, and Cl 3p orbitals to the unoccupied terpyridyl N 2p, C 2p, and Pt 5d orbitals. These calculations also predict a red-shift of the overall spectra of the $[Pt(tpy)Cl]ClO_4$·H_2O trimer systems in comparison to that of the $[Pt(tpy)Cl]PF_6$ trimer system (Figure 4C), indicating that the shorter Pt···Pt contacts in the $[Pt(tpy)Cl]ClO_4$·H_2O are a contributing factor in the relative energies of the MMLCT transition. The composite simulated spectra of the $[Pt(tpy)Cl]PF_6$ and $[Pt(tpy)Cl]ClO_4$·H_2O trimer systems (Figure 4C) are in reasonable agreement with the $[Pt(tpy)Cl]PF_6$/$[Pt(tpy)Cl]ClO_4$·H_2O absorption spectra of Taylor et al.,[25] and the calculated transition at 520 nm is close to the MMLCT charge-transfer energy of 529 nm found by Taylor et al.[25] We also note that discrepancies in the calculated results compared to the experimental measurements can be possibly attributed to the use of the PBE DFT functional for the geometry optimization,

DOI: 10.1021/acs.inorgchem.5b01664
Inorg. Chem. 2015, 54, 9914–9923

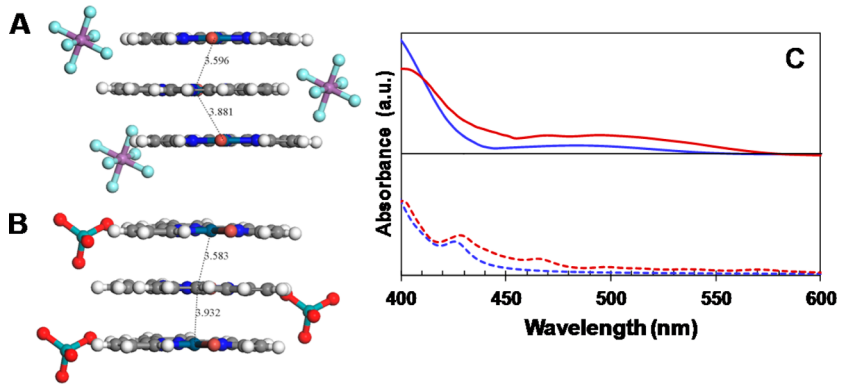

Figure 5. Cluster models of the 1^+ complex systems (A) **1**·SbF_6, (B) **1**·TcO_4. (C) Solid lines: Experimental absorption spectra of the $[Pt(tpy)Br]^+$ systems. Dashed lines: TD-DFT simulated singlet absorption spectra from the trimer model systems. Blue line is for $[Pt(tpy)Br]SbF_6$ absorption, and red line is for $[Pt(tpy)Br]TcO_4$ absorption.

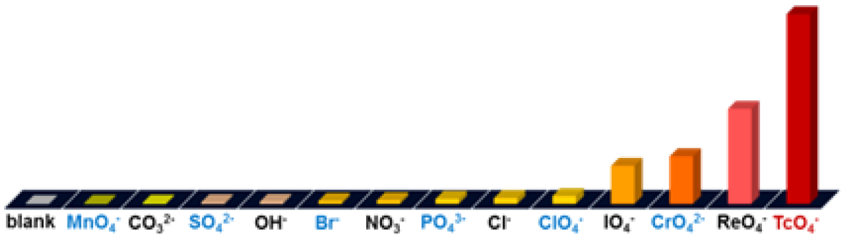

blank	MnO_4^-	CO_3^{2-}	SO_4^{2-}	OH^-	Br^-	NO_3^-	PO_4^{3-}	Cl^-	ClO_4^-	IO_4^-	CrO_4^{2-}	ReO_4^-	TcO_4^-
0.0003	0.0007	0.0008	0.0010	0.0013	0.002	0.005	0.006	0.01	0.02	0.2	0.25	0.5	1

Figure 6. (Top) Bar chart showing the relative selectivity of **1**·SbF_6-loaded Vycor beads toward different anions. (Bottom) Table showing the selectivity factors calculated as the ratio of the maximum emission intensity of **1**·SbF_6-loaded Vycor beads measured in the presence of competing anions to that observed in the presence of TcO_4^-.

which is known to overestimate bond and lattice lengths,[75,76] the use of a finite cluster, and the use of a single cluster configuration for the UV–vis TDDFT calculations. In reality, it is quite possible that there are several cluster configurations, close in energy, that can contribute to the spectrum. These configurations can be sampled, in principle, via *ab initio* molecular dynamics (AIMD) simulations. Here, we focused on developing a model for this system that is able to capture the dominant features of the experiment, which to the best of our knowledge is a first.

A similar calculation was undertaken for the 1^+ complex, as well as the trimer cluster models derived from the crystal structures of **1**·SbF_6 and **1**·TcO_4 (Figure 5). The Pt···Pt distances for the $[Pt(tpy)Br]^+$ complexes are a little longer than those of the $[Pt(tpy)Cl]^+$ complexes, and therefore the simulated absorption spectra of the $[Pt(tpy)Br]^+$ complexes (Figure 5C), though qualitatively similar to the $[Pt(tpy)Cl]^+$ complexes, are predicted to be blue-shifted. The feature at 438 nm in the spectrum of the **1**·SbF_6 system corresponds to singlet–singlet transitions from a mixture of Pt d and ligand π orbitals to unoccupied Pt d and ligand π orbitals. An analogous band is predicted in the spectrum of **1**·TcO_4 peak near 439 nm, corresponding to the singlet–singlet transition from the Pt 5d and Br 4p orbitals to the C and N 2p orbitals of the terpyridyl ligand. Because our TDDFT simulated spectra only represent singlet–singlet transitions in the absence of spin–orbit effects, we have also calculated the energies of the spin-forbidden singlet–triplet transitions. Those simulations predict transitions from occupied Pt 5d orbitals to unoccupied Pt 5d and terpyridyl C and N 2p orbitals in the range 438–479 nm, which can be assigned to spin-forbidden MMLCT transitions (Figure 5C). Similar simulation of a hypothetical **1**·TcO_4·H_2O structure shows a red shift in the MMLCT transition as the Pt···Pt distance gets reduced (Figure S9).

TcO_4^- Response. *Selectivity of TcO_4^- Response.* For application of the spectroscopic response to real time detection of aqueous TcO_4^- in environmental samples, selectivity and sensitivity are two important considerations. Vycor glass beads containing **1**·TcO_4·xH_2O showed an intense emission band maximizing at 655 nm (Figure S10, Supporting Information), which can be utilized for the quantification of the TcO_4^- anion. The emission is red-shifted from those of aqueous suspensions (592 nm as shown in Figure S11), presumably due to the unique microenvironment in Vycor. In order to determine the selectivity of the response of **1**·SbF_6 to various anions, beads loaded with **1**·SbF_6 were exposed to the aqueous solutions containing 1.0 mM aqueous solutions of TcO_4^-, ReO_4^-, IO_4^-, ClO_4^-, MnO_4^-, CrO_4^{2-}, Cl^-, PO_4^{3-}, NO_3^-, Br^-, OH^-, CO_3^{2-}, or SO_4^{2-}. This list includes potentially interfering anions commonly present in the groundwater (e.g., Cl^-, PO_4^{3-}, NO_3^-, OH^-, CO_3^{2-}, or SO_4^{2-}) and anions with properties similar to TcO_4^-.

Upon exposure to TcO_4^-, the glass beads exhibited an intense luminescence at 655 nm when irradiated at 532 nm. The emission spectrum is nearly identical to that of **1**·TcO_4·xH_2O in glass beads (Figure S12A, Supporting Information). Glass beads exposed to the other anions showed no or only weak emissions (Figure S12B, Supporting Information). The selectivity factors calculated as the ratio of the maximum emission intensities observed in the presence of competing

DOI: 10.1021/acs.inorgchem.5b01664
Inorg. Chem. 2015, 54, 9914–9923

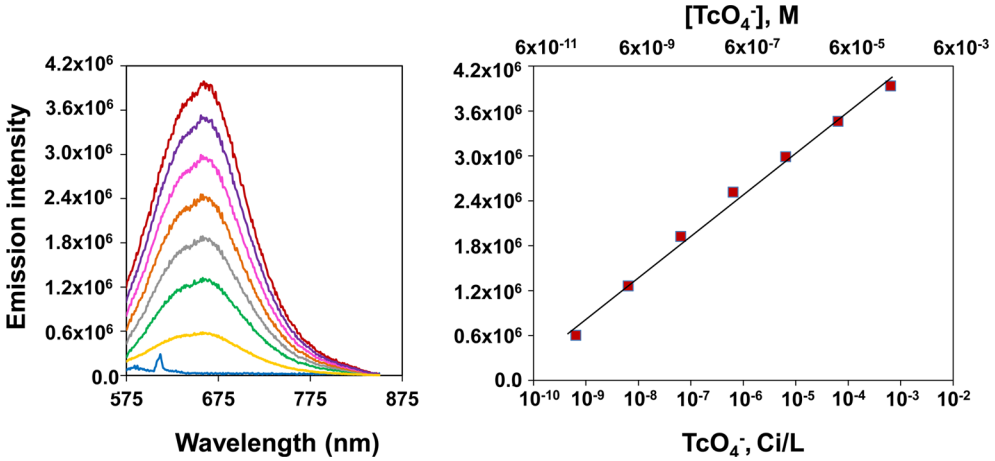

Figure 7. Luminescence spectra (left panel) of **1**·SbF_6 loaded Vycor beads upon exposure to varying concentrations of aqueous TcO_4^- for 1 h: (light blue) 0 M, (yellow) 3.8×10^{-10} M, (green) 3.8×10^{-9} M, (gray) 3.8×10^{-8} M, (orange) 3.8×10^{-7} M, (magenta) 3.8×10^{-6} M, (purple) 3.8×10^{-5} M, (red) 3.8×10^{-4} M (λ_{ex}= 532 nm). Semilogarithmic plot (right panel) of maximum emission intensity (λ_{max}= 655 nm) of the loaded Vycor beads versus the molarity or radioactivity of TcO_4^- in solution shows a linear correlation, with the following equation: emission intensity = $(5.499 \pm 0.002) \times 10^5 \log_{10}[TcO_4^-] + (6.001 \pm 0.003) \times 10^6$; $R^2 = 0.99$. The errors are insignificant compared to the measurements, and therefore, the error bars are avoided in the figure.

anions commonly found in rivers and groundwaters to that observed in the presence of TcO_4^- range from 0.02 (for ClO_4^-) to 0.0008 (for CO_3^{2-}) (Figure 6, bottom table) confirming highly selective TcO_4^- detection. Particularly encouraging are the weak intensities of the response for Cl^-, CO_3^{2-}, SO_4^{2-}, NO_3^-, and PO_4^{3-} as these are the primary anionic components found in a range of drinking water samples across the globe. Also particularly encouraging was the selectivity with respect to perchlorate anion, which is similar in shape and size to TcO_4^-. Together, the results suggest that the hydrated TcO_4^- anions, as compared to Cl^-, CO_3^{2-}, SO_4^{2-}, NO_3^-, and PO_4^{3-}, are particularly well-suited to meet the size and structural and electronic requirements needed to support a continuous chain of stacked square-planar $[Pt(tpy)Br]^+$ cationic units with short Pt···Pt interactions.

While not commonly relevant as potential interfering anions in drinking water samples, other tetraoxy-anions were explored for the generation of **1**·SbF_6 spectroscopic response. Vycor glass beads were loaded with **1**·SbF_6 and exposed to 1.0 mM aqueous solutions of MnO_4^-, CrO_4^{2-}, ClO_4^-, IO_4^-, and ReO_4^-. The emission spectra upon exposure to these anions are shown in Figure S13. For the material exposed to MnO_4^-, no emission was observed when excited at 532 nm, presumably due to quenching of emission by MnO_4^-. Exposure to CrO_4^{2-} resulted in a luminescence band whose maximum was shifted to shorter wavelength compared to that in the presence of aqueous TcO_4^-. Exposure to IO_4^- and ReO_4^-, however, resulted in emission bands with maxima at 647 and 642 nm, respectively, though the intensities were significantly lower than the intensity generated upon exposure to an equally concentrated solution of aqueous TcO_4^- (selectivity factors for competing anions relative to TcO_4^-: IO_4^-, 0.2; ReO_4^-, 0.5). This is suggestive that the "turning on" of the emission of **1**·SbF_6 at longer wavelengths is not exclusive for aqueous TcO_4^- alone, and other oxy-anions with similar shape, size, geometry, chemical nature, and electronic structure can also satisfy the lattice requirements needed for extended Pt···Pt overlap. These results are reassuring in that the observed changes are selective specifically for the aqueous pertechnetate anion and not just due to the phenomenon of water incorporation into the structure resulting in a simple hydrogen-bonding interplay in the solid state. In fact, the observed changes are dependent on certain structural parameters of the anions involved.

In order to assess the response of this material to aqueous TcO_4^- in groundwater samples containing species that can potentially interfere with TcO_4^- measurements (nitrate, chloride, carbonate, as well as uranium-containing species), water from the well 299-W19-36, U.S. DOE Hanford Site, WA (at pH = 7.8, and containing a variety of interfering species listed in Table S2) was used. Vycor glass beads loaded with equal amounts of **1**·SbF_6 (~2% by weight) were exposed for 1 h to groundwater solutions spiked with two different concentrations of TcO_4^- (7.5×10^{-6} and 7.5×10^{-4} M). Upon subsequent excitation at 532 nm, the TcO_4^- exposed Vycor glass beads showed the characteristic 655 nm emission whose intensity increased with the increasing TcO_4^- concentration (Figure S14). This result suggests that **1**·SbF_6 may have practical application in the detection of TcO_4^- in groundwater.

Quantification of TcO_4^- in Water. To test whether the emission intensity can be used for the quantification of the aqueous TcO_4^-, Vycor glass beads loaded with equal amounts of **1**·SbF_6 were exposed for 1 h to aqueous solutions spiked with different concentrations of TcO_4^- ranging from $3.8 \times 10^{-10} - 3.8 \times 10^{-4}$ M corresponding to ^{99}Tc radioactivity of $6.4 \times 10^{-10} - 6.4 \times 10^{-4}$ Ci/L. Upon excitation at 532 nm, the intensity of the characteristic 655 nm emission progressively increased with the increasing TcO_4^- concentration. A working curve of the emission intensity (at 655 nm) as a function of the logarithm of TcO_4^- concentration shows a linear dependence for the entire TcO_4^- concentration range tested (Figure 7, right panel).

A detection limit of 2.6×10^{-10} M or 450 pCi/L in the radioactivity units was determined for aqueous TcO_4^- with the given configuration. This value is below the ^{99}Tc drinking water standard of 900 pCi/L established by the U.S. Environmental Protection Agency.[77] Furthermore, groundwater collected from the well 299-W19-36 at the Hanford site, spiked with 7.5×10^{-8} to 7.5×10^{-6} M of TcO_4^-, showed the characteristic 655 nm emission, illustrating that this configuration holds promise as environmentally deployable sensors for TcO_4^- detection.

DOI: 10.1021/acs.inorgchem.5b01664
Inorg. Chem. 2015, 54, 9914−9923

CONCLUSIONS

This investigation demonstrates for the first time the use of a readily available Pt(II) solid material for the rapid and selective detection of TcO_4^- in aqueous solution. The accumulated data suggest that this material has potential for development of a field deployable and highly selective sensor. The colorimetric and luminescence response of **1**·SbF_6 to aqueous TcO_4^- is a consequence of the enhancement of intermolecular Pt···Pt interactions upon formation of **1**·TcO_4·xH_2O hydrated complex. It appears that the resulting **1**·TcO_4·xH_2O exhibits unique spectroscopic signature that allows for the selective excitation of this material at long wavelengths. The remarkable specificity of this system suggests that stabilization of the MMLCT state and the appearance of intense red emission requires electronic and structural complementarity between the cationic Pt(II) complex and the anion. Overall, the results suggest a novel strategy for TcO_4^- sensing without separation, concentration, or other pretreatment steps.

ASSOCIATED CONTENT

Supporting Information

The Supporting Information is available free of charge on the ACS Publications website at DOI: 10.1021/acs.inorgchem.5b01664.

Crystal structure information on of **1**·TcO_4, composition table of groundwater from well 299-W19-36 at Hanford, WA, and additional spectroscopic and microscopic data (PDF)

X-ray crystallographic data for **1**·TcO_4 (CIF)

AUTHOR INFORMATION

Corresponding Authors

*E-mail: Sayandev.Chatterjee@pnnl.gov.
*E-mail: connicwb@ucmail.uc.edu.
*E-mail: Tatiana.Levitskaia@pnnl.gov.

Notes

The authors declare no competing financial interest.

ACKNOWLEDGMENTS

This research was supported by (1) the Laboratory Directed Research and Development Program at the Pacific Northwest National Laboratory operated by Battelle for the U.S. Department of Energy under Contract DE-AC05-76RL01830 and (2) the National Science Foundation (CHE-1152853), as well as a to A.E.N. (US EPA STAR, FP-91765901). The initial scoping experiments for the selection of the appropriate platinum complex were performed under support from the Office of Science, BER (Grant No. DE-FG02-07ER64353), and the Office of Environmental Management Sciences Program (Grant No. DE-FG0799ER62331) of the U.S. Department of Energy. Part of this research was performed at EMSL, a national scientific user facility at PNNL managed by the Department of Energy's Office of Biological and Environmental Research. We thank Dr. Zheming Wang for helping with spectroscopy measurements and Mr. Paul Macfarlan for helping with SEM measurements. TEA-S was supported by the U.S. Department of Energy, Office of Science, Office of Basic Energy Sciences, Heavy Elements Chemistry Program, under Award Number DE-FG02-13ER16414.

REFERENCES

(1) Steed, J. W. *Chem. Soc. Rev.* **2009**, *38*, 506−519.
(2) Sessler, J. L.; Gross, D. E.; Cho, W. S.; Lynch, V. M.; Schmidtchen, F. P.; Bates, G. W.; Light, M. E.; Gale, P. A. *J. Am. Chem. Soc.* **2006**, *128*, 12281−12288.
(3) Sessler, J. L.; Camiolo, S.; Gale, P. A. *Coord. Chem. Rev.* **2003**, *240*, 17−55.
(4) Gale, P. A. *Coord. Chem. Rev.* **2003**, *240*, 191−221.
(5) Sessler, J. L.; Gale, P. A.; Cho, W. S. *Anion Receptor Chemistry*; Royal Society of Chemistry: Cambridge, U.K., 2006.
(6) Sessler, J. L.; Sansom, P. I.; Andrievsky, A.; Kral, V. In *Supramolecular Chemistry of Anions*; Bianchi, A., Bowman-James, K., Eds.; Wiley-VCH: New York,1997.
(7) Beer, P. D.; Drew, M. G. B.; Hesek, D.; Shade, M.; Szemes, F. *Chem. Commun.* **1996**, 2161−2162.
(8) Perez, J.; Riera, L. *Chem. Soc. Rev.* **2008**, *37*, 2658−2667.
(9) O'Hara, M. J.; Burge, S. R.; Grate, J. W. *Anal. Chem.* **2009**, *81*, 1068−1078.
(10) Seliman, A. F.; Helariutta, K.; Wiktorowicz, S. J.; Tenhu, H.; Harjula, R. *J. Environ. Radioact.* **2013**, *126*, 156−164.
(11) DeVol, T. A.; Egorov, O. B.; Roane, J. E.; Paulenova, A.; Grate, J. W. *J. Radioanal. Nucl. Chem.* **2001**, *249*, 181−189.
(12) Chatterjee, S.; Del Negro, A. S.; Edwards, M. K.; Bryan, S. A.; Kaval, N.; Pantelic, N.; Morris, L. K.; Heineman, W. R.; Seliskar, C. J. *Anal. Chem.* **2011**, *83*, 1766−1772.
(13) Chatterjee, S.; Del Negro, A. S.; Smith, F. N.; Wang, Z. M.; Hightower, S. E.; Sullivan, B. P.; Heineman, W. R.; Seliskar, C. J.; Bryan, S. A. *J. Phys. Chem. A* **2013**, *117*, 12749−12758.
(14) Chatterjee, S.; Bryan, S. A.; Seliskar, C. J.; Heineman, W. R. *Rev. Anal. Chem.* **2013**, *32*, 209−224.
(15) Chatterjee, S.; Del Negro, A. S.; Wang, Z. M.; Edwards, M. K.; Skomurski, F. N.; Hightower, S. E.; Krause, J. A.; Twamley, B.; Sullivan, B. P.; Reber, C.; Heineman, W. R.; Seliskar, C. J.; Bryan, S. A. *Inorg. Chem.* **2011**, *50*, 5815−5823.
(16) Chatterjee, S.; Del Negro, A. S.; Edwards, M. K.; Twamley, B.; Krause, J. A.; Bryan, S. A. *Acta Crystallogr., Sect. E: Struct. Rep. Online* **2010**, *66*, I61−i62.
(17) Del Negro, A. S.; Wang, Z. M.; Seliskar, W. R.; Heineman, W. R.; Sullivan, B. P.; Hightower, S. E.; Hubler, T. L.; Bryan, S. A. *J. Am. Chem. Soc.* **2005**, *127*, 14978−14979.
(18) Del Negro, A. S.; Seliskar, C. J.; Heineman, W. R.; Hightower, S. E.; Bryan, S. A.; Sullivan, B. P. *J. Am. Chem. Soc.* **2006**, *128*, 16494−16495.
(19) Kurz, P.; Probst, B.; Spingler, B.; Alberto, R. *Eur. J. Inorg. Chem.* **2006**, *2006*, 2966−2974.
(20) Briggs, B. N.; McMillin, D. R.; Todorova, T. K.; Gagliardi, L.; Poineau, F.; Czerwinski, K. R.; Sattelberger, A. P. *Dalton T* **2010**, *39*, 11322−11324.
(21) Ikeda, H.; Yoshimura, T.; Ito, A.; Sakuda, E.; Kitamura, N.; Takayama, T.; Sekine, T.; Shinohara, A. *Inorg. Chem.* **2012**, *51*, 12065−12074.
(22) Ikeda, H.; Ito, A.; Sakuda, E.; Kitamura, N.; Takayama, T.; Sekine, T.; Shinohara, A.; Yoshimura, T. *Inorg. Chem.* **2013**, *52*, 6319−6327.
(23) Katayev, E. A.; Kolesnikov, G. V.; Sessler, J. L. *Chem. Soc. Rev.* **2009**, *38*, 1572−1586.
(24) Alberto, R.; Bergamaschi, G.; Braband, H.; Fox, T.; Amendola, V. *Angew. Chem., Int. Ed.* **2012**, *51*, 9772−9776.
(25) Taylor, S. D.; Howard, W.; Kaval, N.; Hart, R.; Krause, J. A.; Connick, W. B. *Chem. Commun.* **2010**, *46*, 1070−1072.
(26) Arena, G.; Calogero, G.; Campagna, S.; Scolaro, L. M.; Ricevuto, V.; Romeo, R. *Inorg. Chem.* **1998**, *37*, 2763−2769.
(27) Wang, X. H.; Goeb, S.; Ji, Z. Q.; Castellano, F. N. *J. Phys. Chem. B* **2010**, *114*, 14440−14449.
(28) Lai, S. W.; Chan, M. C. W.; Cheung, K. K.; Che, C. M. *Inorg. Chem.* **1999**, *38*, 4262−4267.
(29) Buchner, R.; Cunningham, C. T.; Field, J. S.; Haines, R. J.; McMillin, D. R.; Summerton, G. C. *J. Chem. Soc., Dalton Trans.* **1999**, 711−717.

DOI: 10.1021/acs.inorgchem.5b01664
Inorg. Chem. 2015, 54, 9914−9923

(30) Santoro, A.; Wegrzyn, M.; Whitwood, A. C.; Donnio, B.; Bruce, D. W. *J. Am. Chem. Soc.* **2010**, *132*, 10689−10691.
(31) Hill, M. G.; Bailey, J. A.; Miskowski, V. M.; Gray, H. B. *Inorg. Chem.* **1996**, *35*, 4585−4590.
(32) Kui, S. C. F.; Law, Y. C.; Tong, G. S. M.; Lu, W.; Yuen, M. Y.; Che, C. M. *Chem. Sci.* **2011**, *2*, 221−228.
(33) Bailey, J. A.; Hill, M. G.; Marsh, R. E.; Miskowski, V. M.; Schaefer, W. P.; Gray, H. B. *Inorg. Chem.* **1995**, *34*, 4591−4599.
(34) Field, J. S.; Haines, R. J.; McMillin, D. R.; Summerton, G. C. *J. Chem. Soc. Dalton* **2002**, 1369−1376.
(35) Yam, V. W. W.; Chan, K. H. Y.; Wong, K. M. C.; Zhu, N. Y. *Chem. - Eur. J.* **2005**, *11*, 4535−4543.
(36) *Extended Linear Chain Compounds*; Miller, J. S., Ed.; Plenum Press: New York, 1982; Vol. *1*−*3*.
(37) Day, P. *Inorg. Chim. Acta, Rev.* **1969**, *3*, 81−97.
(38) Thomas, T. W.; Underhill, Ae *Chem. Soc. Rev.* **1972**, *1*, 99−120.
(39) Grove, L. J.; Rennekamp, J. M.; Jude, H.; Connick, W. B. *J. Am. Chem. Soc.* **2004**, *126*, 1594−1595.
(40) Grove, L. J.; Oliver, A. G.; Krause, J. A.; Connick, W. B. *Inorg. Chem.* **2008**, *47*, 1408−1410.
(41) Wadas, T. J.; Wang, Q. M.; Kim, Y. J.; Flaschenreim, C.; Blanton, T. N.; Eisenberg, R. *J. Am. Chem. Soc.* **2004**, *126*, 16841−16849.
(42) Kato, M.; Omura, A.; Toshikawa, A.; Kishi, S.; Sugimoto, Y. *Angew. Chem., Int. Ed.* **2002**, *41*, 3183−3185.
(43) Muro, M. L.; Daws, C. A.; Castellano, F. N. *Chem. Commun.* **2008**, 6134−6136.
(44) Exstrom, C. L.; Pomije, M. K.; Mann, K. R. *Chem. Mater.* **1998**, *10*, 942−945.
(45) Exstrom, C. L.; Sowa, J. R.; Daws, C. A.; Janzen, D.; Mann, K. R.; Moore, G. A.; Stewart, F. F. *Chem. Mater.* **1995**, *7*, 15−17.
(46) Yu, C.; Wong, K. M. C.; Chan, K. H. Y.; Yam, V. W. W. *Angew. Chem., Int. Ed.* **2005**, *44*, 791−794.
(47) Yam, V. W. W.; Wong, K. M. C.; Zhu, N. Y. *J. Am. Chem. Soc.* **2002**, *124*, 6506−6507.
(48) Tam, A. Y. Y.; Wong, K. M. C.; Wang, G. X.; Yam, V. W. W. *Chem. Commun.* **2007**, 2028−2030.
(49) Goshe, A. J.; Steele, I. M.; Bosnich, B. *Inorg. Chim. Acta* **2004**, *357*, 4544−4551.
(50) Crowley, J. D.; Steele, I. M.; Bosnich, B. *Inorg. Chem.* **2005**, *44*, 2989−2991.
(51) Mcdermott, J. X.; White, J. F.; Whitesides, G. M. *J. Am. Chem. Soc.* **1976**, *98*, 6521−6528.
(52) Annibale, G.; Brandolisio, M.; Pitteri, B. *Polyhedron* **1995**, *14*, 451−453.
(53) Taylor, S. D. Ph.D. Dissertation, University of Cincinnati, 2011.
(54) Vanderbilt, D. *Phys. Rev. B: Condens. Matter Mater. Phys.* **1990**, *41*, 7892−7895.
(55) Giannozzi, P.; Baroni, S.; Bonini, N.; Calandra, M.; Car, R.; Cavazzoni, C.; Ceresoli, D.; Chiarotti, G. L.; Cococcioni, M.; Dabo, I.; Dal Corso, A.; de Gironcoli, S.; Fabris, S.; Fratesi, G.; Gebauer, R.; Gerstmann, U.; Gougoussis, C.; Kokalj, A.; Lazzeri, M.; Martin-Samos, L.; Marzari, N.; Mauri, F.; Mazzarello, R.; Paolini, S.; Pasquarello, A.; Paulatto, L.; Sbraccia, C.; Scandolo, S.; Sclauzero, G.; Seitsonen, A. P.; Smogunov, A.; Umari, P.; Wentzcovitch, R. M. *J. Phys.: Condens. Matter* **2009**, *21*, 395502.
(56) Monkhorst, H. J.; Pack, J. D. *Phys. Rev. B* **1976**, *13*, 5188−5192.
(57) Perdew, J. P.; Burke, K.; Ernzerhof, M. *Phys. Rev. Lett.* **1996**, *77*, 3865−3868.
(58) Grimme, S. *J. Comput. Chem.* **2006**, *27*, 1787−1799.
(59) Adamo, C.; Barone, V. *J. Chem. Phys.* **1999**, *110*, 6158−6170.
(60) Hariharan, P. C.; Pople, J. A. *Theoret. Chimica. Acta* **1973**, *28*, 213−222.
(61) Francl, M. M.; Petro, W. J.; Hehre, W. J.; Binkley, J. S.; Gordon, M. S.; DeFrees, D. J.; Pople, J. A. *J. Chem. Phys.* **1982**, *77*, 3654−3665.
(62) Bergner, A.; Dolg, M.; Kuechle, W.; Stoll, H.; Preuss, H. *Mol. Phys.* **1993**, *80*, 1431−1441.
(63) Kaupp, M.; Schleyer, P. v. R.; Stoll, H.; Preuss, H. *J. Chem. Phys.* **1991**, *94*, 1360−1366.
(64) Valiev, M.; Bylaska, E. J.; Govind, N.; Kowalski, K.; Straatsma, T. P.; Van Dam, H. J. J.; Wang, D.; Nieplocha, J.; Apra, E.; Windus, T. L.; de Jong, W. W. *Comput. Phys. Commun.* **2010**, *181*, 1477−1489.
(65) Long, G. L.; Winefordner, J. D. *Anal. Chem.* **1983**, *55*, A712−A724.
(66) Mattigod, S. V.; Wellman, D. M.; Golovich, E. C.; Cordova, E.; Smith, R. M. *Tc-99 Adsorption on Selected Activated Carbons*; Pacific Northwest National Laboratory: Richland, WA, 2010.
(67) Taylor, S. D.; Norton, A. E.; Hart, R. T.; Abdolmaleki, M. K.; Krause, J. A.; Connick, W. B. *Chem. Commun.* **2013**, *49*, 9161−9163.
(68) Mckee, D. E.; Adams, C. J.; Bartlett, N. *Inorg. Chem.* **1973**, *12*, 1722−1725.
(69) Mazej, Z.; Goreshnik, E.; Arcon, I.; Logar, N. Z.; Kaucic, V. Z. *Z. Anorg. Allg. Chem.* **2010**, *636*, 224−229.
(70) Busey, R. H.; Keller, O. L. *J. Chem. Phys.* **1964**, *41*, 215−225.
(71) Yip, H. K.; Cheng, L. K.; Cheung, K. K.; Che, C. M. *J. Chem. Soc., Dalton Trans.* **1993**, 2933−2938.
(72) Du, P. W. *Inorg. Chim. Acta* **2010**, *363*, 1355−1358.
(73) Yang, Q. Z.; Wu, L. Z.; Wu, Z. X.; Zhang, L. P.; Tung, C. H. *Inorg. Chem.* **2002**, *41*, 5653−5655.
(74) Paw, W.; Cummings, S. D.; Mansour, M. A.; Connick, W. B.; Geiger, D. K.; Eisenberg, R. *Coord. Chem. Rev.* **1998**, *171*, 125−150.
(75) Haas, P.; Tran, F.; Blaha, P. *Phys. Rev. B: Condens. Matter Mater. Phys.* **2009**, *79*, 85104.
(76) Csonka, G. I.; Perdew, J. P.; Ruzsinszky, A.; Philipsen, P. H. T.; Lebegue, S.; Paier, J.; Vydrov, O. A.; Angyan, J. G. *Phys. Rev. B: Condens. Matter Mater. Phys.* **2009**, *79*, 155107.
(77) U.S. EPA. *EPA Facts About Technetium-99*; 2002. Retrieved April 8, 2014, from http://www.epa.gov/superfund/health/contaminants/radiation/pdfs/technetium.pdf.

DOI: 10.1021/acs.inorgchem.5b01664
Inorg. Chem. 2015, 54, 9914−9923